ARTICLE

Anchoring-mediated topology signature of self-assembled elastomer undergoing mechanochromic coupling/decoupling

Received 00th January 20xx,
Accepted 00th January 20xx

DOI: 10.1039/x0xx00000x

Ziyu Xing[a], Haibao Lu*[a] and Yong Qing Fu*[b]

Soft elastomers with their abilities to integrate strain-adaptive stiffening and coloration have recently received significant research interests for applications in artificial muscle and active camouflage. However, there lacks a theoretical understanding of their complexly molecular dynamics and mechanochromic coupling/decouping. In this study, a topological dynamics model is proposed to understand the anchoring-mediated topology signature of self-assembled elastomers. Based on the constrained molecular junction model, a free-energy function is firstly formulated to describe the working principles of strain-adaptive stiffening and coloration in the self-assembled elastomer. A coupled ternary "rock-paper-scissors" model is proposed to describe the topological dynamics of self-assembly, mechanochromic coupling and mechanoresponsive stiffening of the self-assembled elastomers, in which there are three fractal geometry components in the topology network. Finally, the proposed models are verified using the experimental results reported in literature. This study provides a fundamental approach to understand the working mechanism and topological dynamics in the self-assembled elastomers, with molecularly encoded stiffening and coloration.

1 Introduction

Elastomer, one of the most popular soft matters, has been widely used for sensors,[1,2] wound dressing,[3] piezoelectric devices and artificial muscles,[4,5] attributed to their abilities to integrate adaptive coloration and mechanical properties.[6] Mechanochromic properties of the elastomers enable them with great potentials in applications of biological tissues and living organisms such as chameleons.[7-9] Furthermore, great effort has been made in order to achieve good mechanical properties through molecular interactions,[8-12] and to improve biocompatibility[13,14] and stimulus-responsibility.[15,16] However, there are few theoretical investigations or models to understand the working mechanisms and design principles for molecular self-assembly, which are essential for the guidance of chemical synthesis, understanding of structure-property relationships and practical applications.[17-22]

So far, much effort has been made to enhance the mechanical properties of elastomers, e.g., using multi-networks[6,16] and self-assembly methods.[8,9] Previously Davis et al. has successfully made mechanochemical polymers, which have the capability of translating macroscopic forces into chemical reactions by covalently connecting mechanophore molecules to polymers.[23] Most of these studies are focused on the optimization of elastomers' mechanical properties by designing the self-assembly of polymer networks using different components and compositions.[8-16,24-28]

Recently, chameleon-like elastomers have been fabricated through molecularly encoding strain-adaptive stiffening and coloration, and their functional properties can be regulated by the polymer network of self-assembled macromolecules.[9] However, topological dynamics, which plays an essential role to determine the microstructures and macroscale properties of these self-assembled elastomers, has not been well investigated. Furthermore, modelling the couplings of multi-fields has not been widely studied due to the extremely complex constitutive relationships.

In this work, a ternary "rock-paper-scissors" model is employed to characterize the anchoring-mediated topology signature of the self-assembled elastomers, of which the topology network synchronously undergoes topological dynamics of self-assembly, mechanochromic coupling and mechanoresponsive stiffening. Based on the constrained molecular junction model, a free-energy function is formulated to identify the topological dynamics and coupling effect in these self-assembled elastomers. The constitutive relationships are then proposed to predict the mechanoresponsive stiffening and mechanochromic coupling/decoupling. Finally, the proposed models are verified using the experimental results reported in the literature.

2. Theoretical framework

The topological structure of a cross-linked network has a decisive influence on the mechanical properties of polymer. As the elastomers were synthesized through the self-assembly of

[a] State Key Laboratory of Science and Technology on Advanced Composites in Special Environments, Harbin Institute of Technology, Harbin 150080, P.R. China.
[b] Smart Materials and Surfaces Laboratory, Faculty of Engineering and Environment, Northumbria University, Newcastle upon Tyne NE1 8ST, UK.
† E-mail: luhb@hit.edu.cn and richard.fu@northumbria.ac.uk

triblock copolymers, the dynamic networks therefore had various topology signatures due to the increase in numbers of chains involved as shown in Fig. 1. Self-assembly of triblock copolymers yields cross-linked networks, which show the topological network junctions (ψ) of ψ=2, ψ=3, ψ=4 and ψ=6. For example, ψ=3 means that there are three chains self-assembled into a crosslink point in the network. Therefore, the regular hexagon network is formed due to a large number of chains self-assembled to form the network, in which one crosslink point is incorporated of three chains.

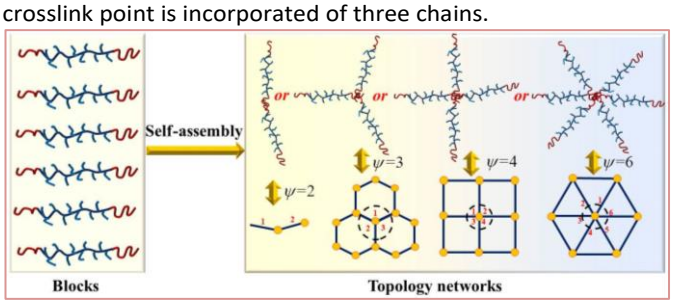

Fig. 1 Illustration of cross-linked topology networks in terms of self-assembly of triblock copolymers in elastomers.

To explore the working principles and topological dynamics of cross-linked network, the elastic free-energy function (ΔF_{el}) is introduced based on the constrained junction model,[29-31]

$$\Delta F_{el} = \Delta F_{ph} + \Delta F_c \quad (1)$$

$$\Delta F_{ph} = \frac{1}{2}(1-\frac{2}{\psi})N_{el}k_BT(\lambda_1^2+\lambda_2^2+\lambda_3^2-3) \quad (2)$$

$$\Delta F_c = \frac{1}{\psi}N_{el}k_BT\sum_i[B_i + D_i - \ln(B_i+1) - \ln(D_i+1)] \quad i=1,2,3 \quad (3)$$

$$B_i = \frac{\kappa_c^2(\lambda_i^2-1)}{(\lambda_i^2+\kappa_c)^2} \quad (4)$$

$$D_i = \frac{\kappa_c\lambda_i^2(\lambda_i^2-1)}{(\lambda_i^2+\kappa_c)^2} \quad (5)$$

where ΔF_{ph} is the free-energy of the phantom network, ΔF_c is the constraint free-energy, ψ is the average functionality of the network junctions, N_{el} is the cross-linking density of elastic phantom network, T is the temperature, k_B is the Boltzmann constant, B_i and D_i are two parameters representing the degrees of the constraints, κ_c is a given parameter for the entanglement constraint in the phantom network, λ_1 , λ_2 and λ_3 represent the stretching ratios of the elastomers along three directions, respectively. According to this constrained junction model,[29-31] the mechanical properties of the elastomer can be described using the parameter,

$$\lim_{\kappa_c\to 0} B_i = 0 \;\&\; \lim_{\kappa_c\to 0} D_i = 0 \quad (6a)$$

$$\lim_{\kappa_c\to 0}\Delta F_{el} = \Delta F_{ph} = \frac{1}{2}(1-\frac{2}{\psi})N_{el}k_BT(\lambda_1^2+\lambda_2^2+\lambda_3^2-3) \quad (6b)$$

$$\lim_{\kappa_c\to \infty} B_i = \lambda_i^2 - 1 \;\&\; \lim_{\kappa_c\to \infty} D_i = 0 \quad (7a)$$

$$\lim_{\kappa_c\to \infty}\Delta F_{el} = N_{el}k_BT[\frac{1}{2}(\lambda_1^2+\lambda_2^2+\lambda_3^2-3) - \frac{2}{\psi}\ln\lambda_1\lambda_2\lambda_3] \quad (7b)$$

Equation (6) can be used to describe the mechanical properties of the elastomer that is governed by the free-energy of the phantom network (ΔF_{ph}), where the weak constraint ($\kappa_c\to 0$) results in ΔF_c=0. Meanwhile, equation (7) is used for describing mechanical properties of the elastomer that is governed by the elastic free-energy function (ΔF_{el}), where the strong constraint ($\kappa_c\to\infty$) results in $\Delta F_c\neq 0$.[29-31] To simplify the expressions of equations (6) and (7), the function of $I_3=\lambda_1\lambda_2\lambda_3=(\mathbf{h}\cdot\mathbf{h}/h_0^2)^{0.5}$ ($\mathbf{h}$ is the tensor of end-to-end distance of a polymer chain and h_0 is the initial end-to-end distance of polymer chain) is introduced, as reported in Refs. [24-31]. Under a uniaxial tension (e.g., $\lambda_1=\lambda$ and $\lambda_2=\lambda_3=(I_3/\lambda)^{0.5}$ where $\lambda_1=\lambda$ is the uniaxial elongation ratio), the constitutive relationship of true stress for the elastomer as a function of elongation ratio can be written as,

$$\sigma_{true} = \lambda\frac{\partial\Delta F_{el}}{\partial\lambda} = N_{el}k_BT[(\lambda^2 - \frac{I_3}{\lambda} + \frac{\partial I_3}{\partial\lambda}) - \frac{2\lambda}{\psi}\frac{\partial I_3/\partial\lambda}{I_3}] + p \quad (8)$$

where p is the hydrostatic pressure. According to the rubber elasticity theory,[17] the change of end-to-end distance (Δh and $|\mathbf{h}|=\Delta h+h_0$) of the polymer chains caused by the external force (f) can be written as,

$$f = \frac{3k_BT}{h_0^2}\Delta h \quad (9)$$

$$f = E_f(\lambda - \frac{1}{\lambda^2}) = 3G_f(\lambda - \frac{1}{\lambda^2}) \quad (10)$$

where E_f is the modulus of the polymer chain.[17] According to the rubber elasticity theory, there is a constitutive relationship between modulus (E_f) and shear modulus (G_f) of $E_f\approx 3G_f$, because the Poisson's ratio is approximately 0.5. Based on the boundary conditions of $\sigma_{true}(\lambda=1)=0$, equation (8) can be rewritten as,

$$I_3 = \frac{h_0+\Delta h}{h_0} = 1 + \frac{E_f h_0}{3k_BT}(\lambda - \frac{1}{\lambda^2}) \quad (11a)$$

$$\frac{\sigma_{true}}{N_{el}k_BT} = \lambda^2 - \frac{1}{\lambda} + \frac{E_f h_0}{k_BT}[\frac{1}{\lambda^3} - 1 - \frac{\frac{2}{3\psi}(\lambda+\frac{2}{\lambda^2})}{1+\frac{E_f h_0}{3k_BT}(\lambda-\frac{1}{\lambda^2})} + \frac{2}{\psi}] \quad (11b)$$

Fig. 2 shows the analytical results obtained using equation (11), which are compared with experiment data of EAMA (EA: ethyl acrylate and MA: methyl acrylate) elastomers reported in Ref. [6]. The parameters used in calculations using the equation (11) are $N_{el}E_fh_0$=5.72 MPa, E_fh_0/k_BT=2.2 and ψ=4. The classical rubber elasticity theory mainly includes two models: the phantom model and the affine model.[17] The affine model is the earlier version of the rubber model. Cross-linking points are the main parts in the affine model, and they are randomly distributed and can move in the same proportion according to macroscopic deformation. According to these assumptions, Flory established the affine model based on Gaussian chain (the free energy of the affine network ΔF_{af} = $N_{el}k_BT(\lambda_1^2+\lambda_2^2+\lambda_3^2-3)/2$).[17] It is found that the analytical results obtained from the constrained junction model are in good agreements with the experimental data, if compared with those obtained using the phantom and affine models.[17] The constrained junction model is suitable to characterize the plasticity of the EAMA elastomer due to the distinct differences in mechanical behaviors of two components of EA and MA, besides of rubber elasticity.[6] Furthermore, the contribution of junction to the mechanical behavior has also been considered by the constrained junction model. Whereas for the phantom and affine models, the cross-linking point has not been considered to influence the mechanical

behavior. Therefore, our theoretically analytical results fit well with the experimental ones.

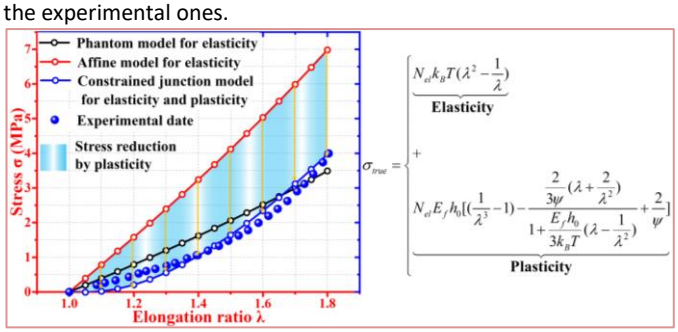

Fig. 2 Comparisons between analytical results using equation (11) and experimental data of the EAMA elastomer reported in Ref. [6], based on the constrained junction, phantom and affine models. During the uniaxial extension, the EAMA elastomer undergoes mechanochemical reaction,[6] and the stretchable network is strongly constrained by the broken chains, which is well predicted by the constrained junction model.

2.1 Topological dynamics and transition

As reported in Ref. [9], PMMA-PDMS-PMMA (PMMA: poly(methylmethacrylate); PDMS: polydimethylsiloxane) elastomers were synthesized through the self-assembly of linear-bottlebrush-linear (PMMA works as the linear block and PDMS acts as the bottlebrush) triblock copolymers. To investigate topological dynamics and mechanochromic coupling, the constitutive relationship between molecular topology structure and mechanochromic property is proposed for the self-assembled elastomers.

According to the interfacial free-energy equation, the free-energy function of microphase (F_A) is introduced as,[22,34-36]

$$\frac{F_A}{k_BT}=\frac{1}{l_{bA}^2}\sqrt{\frac{\chi}{6}}\frac{3N_Al_{bA}^3}{d_2/2}+\frac{3}{2}\frac{d_2^2}{N_Al_{bA}^2} \quad (12)$$

where l_{bA} is the segment length, χ is the interaction parameter, N_A is the segment number and d_2 is the diameter of the self-assembled domain. According to the principle of minimized interfacial free-energy function ($\partial\Delta F_A/\partial d_2$=0), the diameter can then be obtained as,

$$\frac{\partial F_A}{\partial d_2}=0\Rightarrow d_2=(\frac{2\chi}{3})^{\frac{1}{6}}N_A^{\frac{2}{3}}l_{bA} \quad (13)$$

Fig. 3A illustrates the physically cross-linked and topology networks. d_2 is the diameter of spherically shaped PMMA domain. d_3 represents the distance between two PMMA domains and it determines the morphochromism of elastomer, which can be obtained from the ultra-small-angle x-ray scattering (USAXS) measurements. Meanwhile, Fig. 3B describes the working principles of mechanochromic coupling for the self-assembled network. Under a tensile loading, the distance between two PMMA domains (d_3) is gradually decreased due to the increase in the elongation ratio (λ). Therefore, the ternary coupled "rock-paper-scissors ($d_2(h_0)$-$d_3(h_0)$-λ)" model is then employed to describe the topological dynamics and transition of self-assembly, mechanochromic coupling and mechanoresponsive stiffening, in which there are three fractal geometry components in the topology network.[35]

The item of ψ is the average functionality of the network junctions and plays an essential role to determine the microphase separation of PMMA-PDMS-PMMA elastomers.[9] As revealed in Fig. 3, the microphase is originated from spherically shaped PMMA domain, of which the volume is determined by the intra-domain distance (d_2) and obtained from $4/3\pi(d_2/2)^3=\pi(\chi/54)^{0.5}N_A^2l_{bA}^3$, whereas the volume of each chain is $N_Al_{bA}^3$. Based on the Flory-Huggins theory for microphase separation,[20-22] the number of self-assembled chains undergoing the microphase separation can be obtained based on $\psi=\pi(\chi/54)^{0.5}N_A^2l_{bA}^3/N_Al_{bA}^3=\pi(\chi/54)^{0.5}N_A\approx4$, whereas χ=1 and $N_A\approx10.5$.[20-22,32,33]

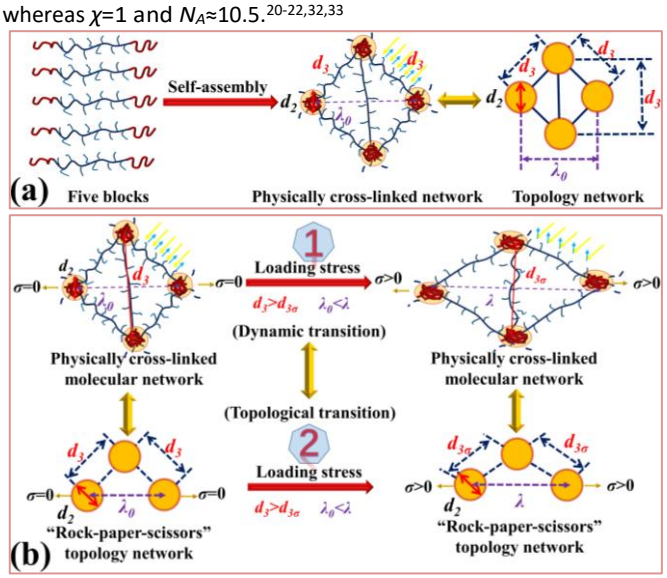

Fig. 3 Schematic illustrations of mechanochromic coupling in terms of domains (d_2 and d_3) and elongation ratio (λ) in elastomer. A) For dynamic transition of molecular networks. B) Topological transition of topology networks.

The mass ratio (<x_β>) of each site is used to characterize the effect of d_2 on the topology network, and it has the following expression,

$$\langle x_\beta\rangle\approx\exp(-\frac{\beta}{2}\ln\frac{1}{d_3-d_2})=(d_3-d_2)^{\frac{\beta}{2}}\quad(\beta=1,2,\ldots,N) \quad (14)$$

where β is the number of domains with a unique diameter of d_2, and N is the number of chains in a spherically shaped domain.

Then, the molecular weight distribution (<M_β>) of the domains is given as,

$$\langle M_\beta\rangle=M_0\langle x_\beta\rangle\ (\beta=1,2,\ldots,N) \quad (15)$$

where M_0 is the molecular weight of one chain.

According to the rubber elastic theory,[17,20] the initial end-to-end distance (h_0) can be then obtained,

$$h_0=\sum_{\beta=1}^{N}\sqrt{\frac{C_{sc}}{N_{el}}}=\sum_{\beta=1}^{N}\frac{C_{sc}}{\frac{\rho N_{Avo}}{M_0\langle x_\beta\rangle}}=\sum_{\beta=1}^{N}\frac{C_{sc}M_0}{\rho N_{Avo}}(d_3-d_2)^{\frac{\beta}{2}} \quad (16)$$

where C_{sc} is a scaling constant, $N_{el}=\rho N_{Avo}/<M>$, $N_{el}h_0^2= C_{sc}$, ρ is the density of the elastomer, N_{Avo} is the Avogadro's constant and $d_2= (2\chi/3)^{1/6}N_A^{2/3}l_{bA}$.

Substituting equations (11) and (13) into (16), the end-to-end distance of a polymer chain (h_0) and the true stress functions can be obtained as,

$$h_0 = \sum_{\beta=1}^{N} \frac{C_{sc}M_0}{\rho N_{Avo}}(d_3 - d_2)^{\frac{\beta}{2}} \approx \frac{C_{sc}M_0}{\rho N_{Avo}}[d_3^{\frac{1}{2}} - (\frac{\chi}{96})^{\frac{1}{6}} l_{bA} d_3^{\frac{-1}{2}} V_A^{\frac{2}{3}} \phi_A^{\frac{2}{3}}] \quad (17a)$$

$$\sigma_{true} = \frac{C_{sc}E_f}{h_0}[\frac{k_BT}{E_f h_0}(\lambda^2 - \frac{1}{\lambda}) + \frac{1}{\lambda^3} - 1 - \frac{\frac{2}{3\psi}(\lambda + \frac{2}{\lambda^2})}{1 + \frac{E_f h_0}{3k_BT}(\lambda - \frac{1}{\lambda^2})} + \frac{2}{\psi}] \quad (17b)$$

where $N_A=V_A\phi_A$, V_A is the number of chains and ϕ_A represents the volume fraction of one chain in the domain.

To verify equation (17b), the analytical results of stress as a function of elongation ratio have been plotted for the elastomer, of which the topology networks undergo dynamic transitions, at a given parameter of E_fh_0/k_BT=2 and $C_{sc}E_f/h_0$=1.0MPa. As shown in Fig. 4A, the constitutive stress-elongation ratio relationship has been investigated at different topological network junctions (ψ) of ψ=2, ψ=3, ψ=4 and ψ=6 for the self-assembled elastomer.

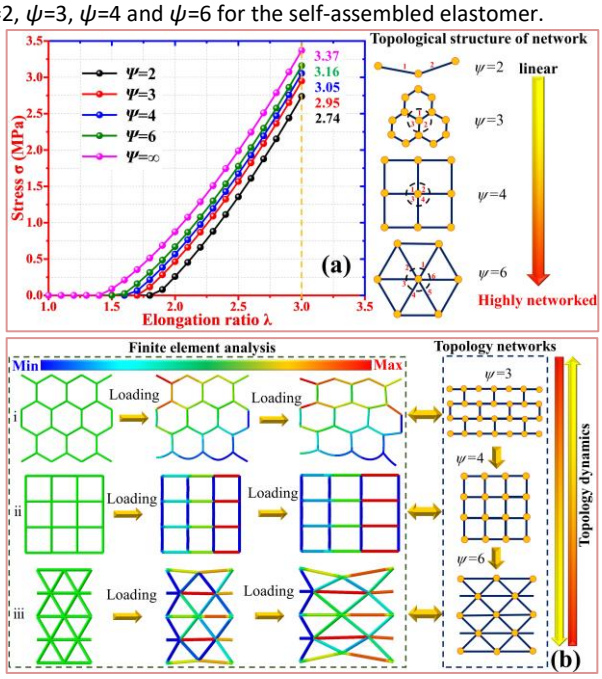

Fig. 4 A) Analytical results based on equation (17) for the stress as a function of elongation ratio of elastomer, at a given constrained junction of ψ=2, 3, 4, 6 and ∞. B) FEA of the dynamic deformation and transition of topology networks, at a given ψ=3, 4 and 6.

With an increase in the junctions (ψ) from ψ=2, ψ=3, ψ=4 to ψ=6 in the topology networks, the stress is gradually increased from 2.74 MPa, 2.95 MPa, 3.05 MPa to 3.16 MPa at the same elongation ratio of λ=3.0. In theoretical analysis, the value of ψ can be infinity, which means each chain is crosslinked to an infinite number of other chains, and the theoretical maximum can help scientists o tdetermine the enhancement effect of physical crosslinking and prevent blind application. These analytical results indicate that the topology structure has a significant influence on the mechanical properties of the self-assembled elastomer, which is attributed to the increased cross-linking density in the polymer network based on the rubber elastic theory.[17,20] On the other hand, the finite-element analysis (FEA) method is also applied to analyze the dynamic transitions of these topology networks, and the obtained results are shown in Fig. 4B. As designed, the mechanical behavior of self-assembled elastomer is critically determined by the constrained junction (ψ), which determines the cross-linking density. With an increase in the constrained junctions from ψ=3, ψ=4 to ψ=6, the mechanical stress of topology network is then gradually increased owing to the increased cross-linking density. According to the constrained junction model,[29-31] topological dynamics of the cross-linked network is resulted from the increased constrained junctions due to the externally mechanical loading, which causes that the topology network shows an enhanced mechanical performance and the elastomer shows a classical plasticity. These analytical results provide a working principle in topological dynamics and transition of self-assembled elastomers, which undergo strain-adaptive stiffening as the experimental results revealed.[9]

2.2 Mechanochromic coupling and decoupling

Optical properties of the elastomer are also determined by the dynamic transition of topology network due to the mechanochromic coupling, where the inter-domain distance (d_3, which is linked with the optical property) is determined by the strain-adaptive elongation ratio (λ, which is linked with the mechanical property).[9] Here, the refractive index (n) can be described as,[36,37]

$$n = n_0\left|\frac{\mathbf{h}\cdot\mathbf{h}}{h_0^2}\right| = n_0[1 + \frac{E_f h_0}{3k_BT}(\lambda - \frac{1}{\lambda^2})]^2 \quad (18)$$

where n_0 is the initial value of refractive index parameter without stress.

To identify the working principles in mechanochromic coupling and decoupling of self-assembled elastomer, the effects of strain-adaptive elongation ratio (λ) on the mechanical stress and optical refractive index have been investigated, and the results are shown in Fig. 5. The analytical results of stress as a function of elongation ratio (λ) have been firstly plotted in Fig. 5A. It is revealed that the stress is gradually increased from 1.94 MPa, 2.45 MPa, 2.89 MPa, 3.62 MPa to 4.63 MPa with an increase in the diameter of spherically shaped domain (d_2) from 30 nm, 35 nm, 40 nm, 45 nm to 50 nm, at a given elongation ratio of λ=3.0. With a given value of the diameter of spherically shaped domain (d_2), the inter-domain distance (d_3), which determines the optical property of elastomer,[9] is decreased with an increase in the elongation ratio (λ). Here the end-to-end distance of a polymer chain (h_0) is decreased, thus resulting in the increase of stress according to the equation (17b). These analytical results can be explained by the rubber elastic theory,[17,20] e.g., the constrained junctions (ψ) is increased with an increase in the diameter of spherically shaped domain (d_2), which results in more chains self-assembled into the domain. Furthermore, the cross-linking density of polymer network is increased to achieve an enhanced mechanical property of the elastomer.

On the other hand, the mechanochromic coupling of the self-assembled polymer network has been further investigated for the

elastomer, and the obtained results are shown in Fig. 5B. Firstly, the analytical results of refractive index as a function of elongation ratio (λ) have been plotted at a given value of $E_f h_0/k_BT$=0.1, 0.2, 0.3, 0.4 and 0.5, in order to identify the working principles of mechanochromic coupling and decoupling during the dynamic transition of topology network. It is revealed that the refractive index is increased from 1.08, 1.28, 1.49, 1.72 to 1.96 with an increase in the $E_f h_0/k_BT$ from 0.1, 0.2, 0.3, 0.4 to 0.5, at a given elongation ratio of λ=3.0. Here the end-to-end distance of a polymer chain (h_0) is kept a constant in order to maintain the value of $E_f h_0/k_BT$ a constant. These analytical results reveal that the refractive index is gradually increased with an increase in the $E_f h_0/k_BT$ from 0.1 to 0.5. The strain-adaptive coloration is determined by the end-to-end distance of a polymer chain (h_0), which is originated from the inter-domain distance (d_3) as the diameter of spherically shaped domain (d_2) is kept a constant. The analytical results can be verified by the experimental ones reported in Ref. [9], in which the strain-adaptive coloration is determined by the inter-domain distance (d_3) based on the experimental USAXS measurements.[9]

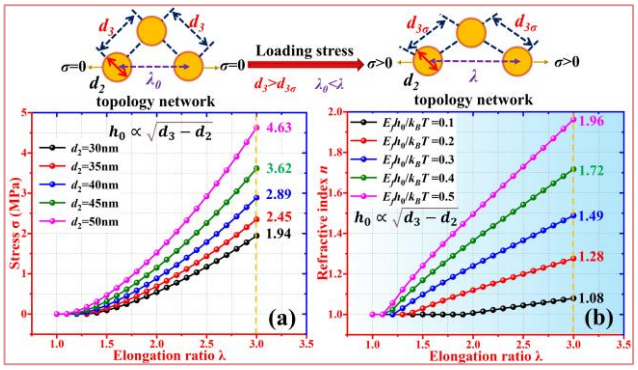

Fig. 5 Mechanochromic coupling and decoupling of self-assembled elastomer. A) Analytical results of equation (17) for the stress as a function of elongation ratio at a given value of d_2=30 nm, 35 nm, 40 nm, 45 nm and 50 nm, whereas $C_{sc}E_f^2/k_BT$=0.5 MPa, ψ=4 and $E_f C_{sc}M_0/N_{Avo}k_BT\rho$=0.2 nm$^{-0.5}$. B) Analytical results of equation (18) for the refractive index as a function of elongation ratio at a given value of $E_f h_0/k_BT$=0.1, 0.2, 0.3, 0.4 and 0.5, whereas n_0=0.9.

According to these analytical results, the mechanochromic coupling can be therefore characterized using our newly proposed model. The mechanochromic decoupling is determined by the strain-adaptive elongation ratio (λ, for the mechanical property) and inter-domain distance (d_3, for the optical property), respectively, whereas the mechanochromic coupling and decoupling are both governed by the "rock-paper-scissors ($d_2(h_0)$-$d_3(h_0)$-λ)" model in the topology network.[35] Furthermore, these analytical results can be verified using the rubber elastic theory and constrained junction model.[17,20,29-31]

3 Experimental verification of self-assembled elastomer

3.1 Constitutive stress-elongation ratio relationship

According to the interfacial free energy and the thermodynamics of microphase separation, ψ=4 can be determined as shown in Section "2.1 Topological dynamics and transition". Moreover, according to equation (17), the nonlinear terms are tended to be constants when λ is large ($1/\lambda^3 \to 0$, $\lambda+2/\lambda^2 \to \lambda$ and $\lambda-1/\lambda^2 \to \lambda$), where the modulus can be estimated according to the end point. After these two parameters are determined, the data can be processed and the remaining two thermodynamic parameters which are difficult to obtain through experiments can be obtained by the least square method.

To experimentally verify the proposed model of equation (17), the analytical results have been plotted in Fig. 6 to predict the mechanical stress-elongation ratios of the PMMA-PDMS-PMMA elastomers,[9] whereas the effect of volume faction of PMMA (ϕ_A) has been investigated at a given segment number of PDMS (N_B). During the analysis, the following parameters are used in equation (17), e.g., $E_f C_{sc}M_0 d_3^{0.5}/N_{Avo}k_BT\rho$=2.2, $E_f C_{sc}M_0\chi^{1/6}l_{bA}V_A^{2/3}/N_{Avo}k_BT\rho d_3^{0.5}$=8.7, ψ=4 and $C_{sc}E_f^2/k_BT$=180 kPa. The obtained analytical results shown in Fig. 6A reveal that the stress is increased from 274 kPa, 361 kPa to 410 kPa, with an increase in the volume faction of PMMA (ϕ_A) from 0.03, 0.06 to 0.17.

Table 1. Comparison between analytical results and experimental data of the maximum true stress in Fig.6.

ϕ_A	σ_{me}(10^5Pa)	σ_{ms}(10^5Pa)	R^2
0.03	4.10	3.23	96.69%
0.06	3.61	2.85	92.94%
0.17	2.74	2.42	92.02%

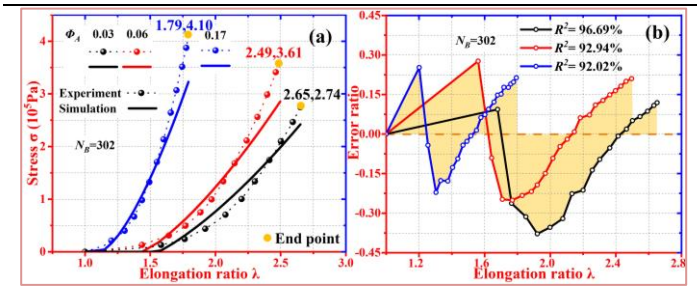

Fig. 6 Comparisons of analytical (using equation (17)) and experimental results for the stress as a function of elongation ratio in PMMA-PDMS-PMMA elastomers with various volume faction of PMMA (ϕ_A) of ϕ_A= 0.03, 0.06 and 0.17, at a given segment number of PDMS (N_B) of N_B=302.[9] A) For the constitutive stress-elongation ratio curves. B) Divergences of the analytical and experimental results.

As discussed above for the topology network of self-assembled elastomers, the increase in volume faction of PMMA (ϕ_A) results in the increased diameter of spherically shaped domain (d_2), and the decreased end-to-end distance of a polymer chain (h_0, $h_0 \propto (d_3-d_2)^{0.5}$). Therefore, the stress is increased due to the decrease in end-to-end distance of a

polymer chain (h_0), based on the equation (17). Furthermore, the divergences between the analytical and experimental results[9] of the PMMA-PDMS-PMMA elastomers are calculated using the correlation index (R^2), which are 96.69%, 92.94% and 92.02% for ϕ_A=0.03, 0.06 and 0.17, respectively, as shown in Fig. 6B. Meanwhile, the comparisons between analytical results and experimental data are listed in Table 1, where σ_{me} is the true stress at the maximum elongation ratio for experimental data and σ_{ms} is the true stress at the maximum elongation ratio for analytical results.

On the other hand, the analytical results of stress as a function of elongation ratio for the PBMA-PDMS-PBMA (PBMA: poly(benzyl methacrylate)) elastomers have been plotted and compared with the experimental results reported in literature.[15] Effects of volume faction of PBMA (ϕ_A) and the chain number of PDMS (N_B) have also been investigated, and the results are shown in Fig. 7.

Table 2. Comparison between analytical results and experimental data of the maximum true stress in Fig.7.

ϕ_A	σ_{me}(10^5Pa)	σ_{ms}(10^5Pa)	R^2
0.05	0.38	0.37	94.76%
0.10	0.72	0.44	84.92%
0.25	0.98	0.95	97.15%

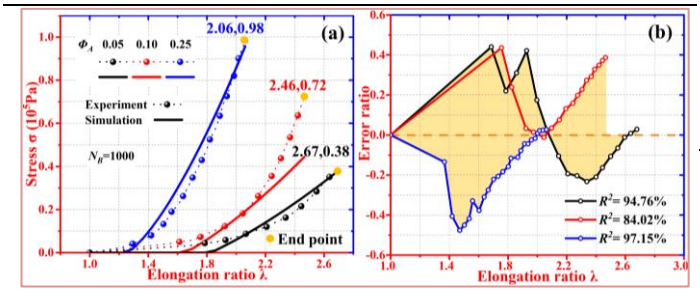

Fig. 7 Comparisons of analytical and experimental results for the stress as a function of elongation ratio in PBMA-PDMS-PBMA elastomers with various volume faction of PBMA (ϕ_A) of ϕ_A=0.05, 0.10 and 0.25, at a given segment number of PDMS (N_B) of N_B=1000.[15] A) For the constitutive stress-elongation ratio curves (using equation (17)). B) Divergences of the analytical and experimental results.

The following parameters are used in equation (17), e.g., $E_fC_{sc}M_0d_3^{0.5}/N_{Avo}k_BT\rho$=3.1, $E_fC_{sc}M_0\chi^{1/6}I_{bA}V_A^{2/3}/N_{Avo}k_BT\rho d_3^{0.5}$=9.9, ψ=4 and $C_{sc}E_f^2/k_BT$=60 kPa. The obtained analytical results show good agreements with the experimental data of self-assembled PBMA-PDMS-PBMA elastomers. It is found that the stress is increased from 38 kPa, 72 kPa to 98 kPa, with an increase in the volume faction of PBMA (ϕ_A) from 0.05, 0.10 to 0.25. As discussed above for the topology network of self-assembled elastomer, the increase in volume faction of PBMA (ϕ_A) results in the increased diameter of spherically shaped domain (d_2) and the decreased end-to-end distance of a polymer chain (h_0, $h_0 \propto (d_3-d_2)^{0.5}$). Therefore, the stress is increased due to the decrease in end-to-end distance of a polymer chain (h_0). The divergences between the analytical and experimental results[15] of the PBMA-PDMS-PBMA elastomer are calculated using the correlation index (R^2), and the results are 94.76%, 84.02% and 97.15% for ϕ_A=0.05, 0.10 and 0.25, respectively, as shown in Fig. 7B. Moreover, the comparisons between the analytical results and experimental data are listed in Table 2.

Effect of the chain number of PMMA (N_A) on the constitutive stress-elongation ratio relationship of the PMMA-PDMS-PMMA elastomers has further been investigated, and the results are shown in Fig. 8. The analytical results have been plotted as a function of elongation ratio in order to predict the experimental results of stress,[9] whereas the chain number of PMMA (N_A) is chosen as 365, 480, 810 and 930. The following parameters are used in the calculation using equation (17), e.g., $E_fC_{sc}M_0d_3^{0.5}/N_{Avo}k_BT\rho$=4.9, $E_fC_{sc}M_0\chi^{1/6}I_{bA}/N_{Avo}k_BT\rho d_3^{0.5}$= 0.06, ψ=4 and $C_{sc}E_f^2/k_BT$=2.8×10^5Pa. The analytical results in Fig. 8A reveal that the stress is decreased from 369 kPa, 297 kPa, 276 kPa to 200 kPa, with an increase in the chain number of PMMA (N_A) from 365, 480, 810 to 930.

Table 3. Comparison between analytical results and experimental data of the maximum true stress in Fig.8.

N_A	σ_{me}(10^5Pa)	σ_{ms}(10^5Pa)	R^2
365	3.69	3.09	93.05%
480	2.97	2.35	90.83%
810	2.76	2.76	91.23%
930	2.00	2.08	94.07%

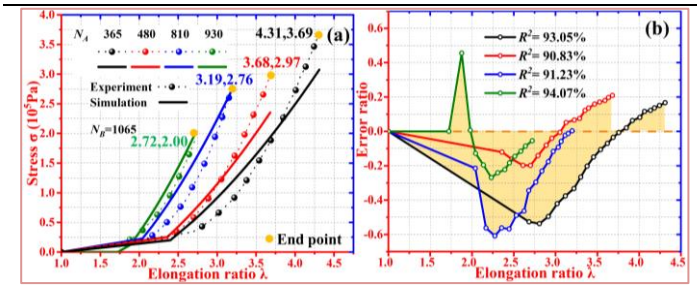

Fig. 8 Comparisons of analytical and experimental results[15] for the stress as a function of elongation ratio in PMMA-PDMS-PMMA elastomers with various segment numbers of PMMA, N_A=365, 480, 810 and 930. A) For the constitutive stress-elongation ratio curves (using equation (17)). B) Divergences of the analytical and experimental results.

As discussed above for the topology network of self-assembled elastomer, increase in the chain number of PMMA (N_A) results in increases of the diameter of spherically shaped domain (d_2), whereas the end-to-end distance of a polymer chain (h_0, $h_0 \propto (d_3-d_2)^{0.5}$) is then decreased as the chain number of PDMS (N_B) is kept at a constant of N_B=1065. With the decrease in the end-to-end distance of a polymer chain (h_0), the modulus is therefore increased as revealed in equation (17). It is worthwhile to note that the high modulus of the self-assembled elastomer is resulted from the smaller value of h_0,

leading to a larger true stress under the same elongation ratio. Meanwhile, the divergences between the analytical and experimental results[9] of the PMMA-PDMS-PMMA elastomers are calculated using the correlation index (R^2), which are 93.05%, 90.83%, 91.23% and 94.07% for N_A=365, 480, 810 and 930, respectively, as shown in Fig. 8B. The comparisons between analytical results and experimental data are listed in Table 3.

3.2 Self-healing behavior in elastomer

The self-healing behavior plays an essential role to determine the mechanical properties of elastomer, where the broken polymer chains produce free radicals and the reaction rates of self-healing (k_h) are governed by the Fick's second diffusion law.[20,21] Therefore, the reaction rate of self-healing (k_h) can be expressed by,

$$\frac{\partial k_h}{\partial t} = D\frac{\partial^2 k_h}{\partial z^2} \tag{19}$$

where t is the time, $D=k_BT/6\pi\eta R_h$ is the diffusion coefficient, z is the distance, R_h is the hydrodynamic radius and η is the viscosity. The value of η can be further expressed as,[21]

$$\eta = \eta_0 N_{ela}^3 \tag{20a}$$

$$N_{ela} = N_0\left\langle x_\beta \right\rangle \tag{20b}$$

where η_0 is the initial viscosity, N_{ela} is the segment number of elastomer and N_0 is initial segment number of the elastomer.

Substituting equations (14) and (20) into $D=k_BT/6\pi\eta R_h$, the diffusion coefficient can be obtained,

$$D = \frac{k_BT}{6\pi\eta_0 R_h N_0^3}\sum_{\beta=1}^{N}(d_3-d_2)^{\frac{-3\beta}{2}} \tag{21}$$

In combination of equations (19) and (21), the reaction rate of self-healing (k_h) of elastomer can be obtained as,

$$k_h = k_{h0} - (k_{h0}-k_{hl})\frac{2}{\sqrt{\pi}}\int_0^{\frac{z}{2\sqrt{Dt}}}\exp(-\frac{z^2}{4Dt})d\frac{z}{2\sqrt{Dt}} \tag{22}$$

where k_{h0} is the initial constant of reaction rate and k_{hl} is the constant of reaction rate under the mechanical loading.

Figure 9 shows the analytical results of self-healing ratios as a function of waiting time, which are also compared with the experimental results reported in Ref. [38,39]. Experimental data of PEA-co-IBA (PEA: phenyl ether acrylate; IBA: isobornyl acrylate) elastomers are used to compare with the analytical results of self-healing ratio as shown in Fig. 9A.[38] The following parameters are used in equations (21) and (22), e.g., k_{h0}=1.1, k_{hl}=0.45, N=11, d_3-d_2=1.1 and $z(3\pi\eta_0R_hN_0^3/2k_BT)^{0.5}$=71.64. While the experimental data of NaSS-co-MPTC (NaSS: sodium p-styrenesulfonate; MPTC: 3-(methacryloylamino) propyltrimethylammonium chloride) elastomers reported in Ref. [39] are used to compare with the analytical results of self-healing ratio, as shown in Fig. 9B, whereas the following parameters are used in equations (21) and (22), e.g., k_{h0}=1.15, k_{hl}=0.2, N=11, d_3-d_2=1.1 and $z(3\pi\eta_0R_hN_0^3/2k_BT)^{0.5}$=58.45. It is found that the analytical results from our models are in good agreements with the experimental data of PEA-co-IBA and NaSS-co-MPTC elastomers, which undergo the self-healing as a function of waiting time. Meanwhile, the divergences between the analytical and experimental results[38,39] of the elastomers are calculated using the correlation index (R^2), which are 93.77% and 99.03% for PEA-co-IBA and NaSS-co-MPTC elastomers, respectively.

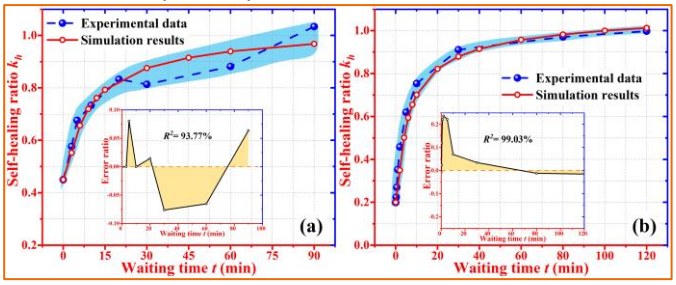

Fig. 9 Comparisons of analytical and experimental results for the self-healing ratio as a function of waiting time.[38,39] A) For the PEA-co-IBA elastomer.[38] B) For the NaSS-co-MPTC elastomer.[39]

4 Conclusions

In this study, we propose a topological dynamic framework to investigate the working principle of strain-adaptive stiffening and coloration in self-assembled elastomers. The anchoring-mediated topology signature is explored to describe the topological dynamics and transition of self-assembly, mechanoresponsive stiffening and mechanochromic coupling, in terms of three fractal geometry components, respectively. A free-energy equation is firstly developed based on the extended constrained molecular junction model, in order to formulate the constitutive stress-elongation ratio relationship, identify the topological dynamics in mechanochromic coupling and decoupling of elastomers, in terms of ternary "rock-paper-scissors ($d_2(h_0)$-$d_3(h_0)$-λ)" model, whereas diameter of domain (d_2) for self-assembly, inter-domain distance (d_3) for morphochromism and elongation ratio (λ) for mechanical elongation. Finally, the proposed framework is proved to be able to well predict topological dynamics, mechanochromic coupling and self-healing behaviors of self-assembled elastomers, and the accuracy of analytical results has then been verified using the experimentally obtained data reported in literature, which have been well fitted. This newly proposed model provides a new mechanism of topology dynamics in self-assembled elastomers and also critical insights into the physical principles which govern the constitutive relationship between molecular self-assembly and mechanochromic coupling.

Conflicts of interest

There are no conflicts to declare.

Author contributions

ZY conceived and designed the analysis, collected data and contributed data and performed the analysis. HB conceived and designed the analysis, performed the analysis and wrote the paper. YQ performed the analysis and wrote the paper.

Acknowledgements

This work was financially supported by the National Natural Science Foundation of China (NSFC) under Grant No. 11725208, and International Exchange Grant (IEC/NSFC/201078), through Royal Society and NFSC.

References

1 C. Wang, K. Hu, C. Zhao, Y. Zou, Y. Liu, X. Qu, D. Jiang, Z. Li, M. R. Zhang and Z. Li, *Small*, 2020, **16**, 1904758.
2 L. Wang, Y. Chen, L. Lin, H. Wang, X. Huang, H. Xue and J. Gao, *Chem. Eng. J.*, 2019, **362**, 89-98.
3 M. Li, J. Chen, M. Shi, H. Zhang, P. X. Ma and B. Guo, *Chem. Eng. J.,* 2019, **375**, 121999.
4 G. Yun, S. Y. Tang, S. Sun, D. Yuan, Q. Zhao, L. Deng, S. Yan, H. Du, M. D. Dickey and W. Li, *Nat. Commun.*, 2019, **10**, 1300.
5 M. Duduta, E. Hajiesmaili, H. Zhao, R. J. Wood and D. R. Clarke, *Proc. Natl. Acad. Sci. U. S. A.*, 2019, **116**, 2476-2481.
6 E. Ducrot, Y. Chen, M. Bulters, R. P. Sijbesma and C. Creton, *Science*, 2014, **344**, 186-189.
7 I. C. Cuthill, W. L. Allen, K. Arbuckle, B. Caspers, G. Chaplin, M. E. Hauber, G. E. Hill, N. G. Jablonski, C. D. Jiggins, A. Kelber, J. Mappes, J. Marshall, R. Merrill, D. Osorio, R. Prum, N. W. Roberts, A. Roulin, H. M. Rowland, T. N. Sherratt, J. Skelhorn, M. P. Speed, M. Stevens, M. C. Stoddard, D. Stuart-Fox, L. Talas, E. Tibbetts and T. Caro, *Science*, 2017, **357**, 6350.
8 M. Vatankhah-Varnosfaderani, W. F. M. Daniel, M. H. Everhart, A. A. Pandya, H. Y. Liang, K. Matyjaszewski, A. V. Dobrynin and S. S. Sheiko, *Nature*, 2017, **549**, 497-501.
9 M. Vatankhah-Varnosfaderani, A. N. Keith, Y. Cong, H. Y. Liang, M. Rosenthal, M. Sztucki, C. Clair, S. Magonov, D. A. Ivanov, A. V. Dobrynin and S. S. Sheiko, *Science*, 2018, **359**, 1509-1513.
10 M. Jacobs, H. Y. Liang, E. Dashtimoghadam, B. J. Morgan, S. S. Sheiko and A. V. Dobrynin, *Macromolecules*, 2019, **52**, 5095-5101.
11 H. Y. Liang, Z. Wang and A. V. Dobrynin, *Macromolecules*, 2019, **52**, 8617-8624.
12 C. Clair, A. Lallam, M. Rosenthal, M. Sztucki, M. Vatankhah-Varnosfaderani, A. N. Keith, Cong Y, H. Y. Liang, A. V. Dobrynin, S. S. Sheiko and D. A. Ivanov, *ACS Macro Lett.*, 2019, **8**, 530-534.
13 H. Y. Liang, G. S. Grest and A. V. Dobrynin, *ACS Macro Lett.*, 2019, **8**, 1328-1333.
14 A. N. Keith, M. Vatankhah-Varnosfaderani, C. Clair, F. Fahimipour, E. Dashtimoghadam, A. Lallam, M. Sztucki, D. A. Ivanov, H. Y. Liang, A. V. Dobrynin and S. S. Sheiko, *ACS Cent. Sci.*, 2020, **6**, 413-419.
15 V. Karimkhani, M. Vatankhah-Varnosfaderani, A. N. Keith, E. Dashtimoghadam, B. J. Morgan, M. Jacobs, A. V. Dobrynin and S. S. Sheiko, *ACS Appl. Polym. Mater.,* 2020, **2**, 1741-1745.
16 T. Matsuda, T. Nakajima and J. P. Gong, *Chem. Mater.*, 2019, **31**, 3766-3776.
17 L. R. G. Treloar, *The physics of rubber elasticity*, Oxford University Press, 1975.
18 A. V. Dobrynin and J. M. Y. Carrillo, *Macromolecules*, 2011, **44**, 140-146.
19 J. M. Y. Carrillo, F. C. MacKintosh and A. V. Dobrynin, *Macromolecules*, 2013, **46**, 3679-3692.
20 P. J. Flory, *Principles of polymer chemistry*, Cornell University Press, 1953.
21 P. G. Gennes, *Scaling concepts in polymer physics*, Cornell University Press, 1979.
22 N. Hadjichristidis, S. Pispas and G. Floudas, *Block Copolymers: Synthetic Strategies, Physical Properties, and Applications*, John Wiley & Sons, Inc. Press, 2003.
23 D. A. Davis, A. Hamilton, J. L. Yang, L. D. Cremar, D. V. Gough, S. L. Potisek, M. T. Ong, P. V. Braun, T. J. Martınez, S. R. White, J. S. Moore and N. R. Sottos, *Nature*, 2009, **459**, 68-72.
24 D. M. Zhong, Y. H. Xiang, J. Liu, Z. Chen, H. F. Zhou, H. H. Yu, S. X. Qu, W. Yang, *Extreme Mechanics Letters*, 2020, **40**, 100926.
25 Y. H. Xiang, D. M. Zhong, P. Wang, T. H. Yin, H. F. Zhou, H. H. Yu, C. Baliga, S. X. Qu and W. Yang, *J. Mech. Phys. Solids*, 2019, **128**, 208-218.
26 Z. Y. Xing, H. B. Lu, M. Hossain, Y. Q. Fu, J. S. Leng and S. Y. Du, *Polymer*, 2020, **186**, 122039.
27 H. B. Lu, Z. Y. Xing, M. Hossain and Y. Q. Fu, *Composites Part B*, 2019, **179**, 107528.
28 X. H. Zhao, *Proc. Natl. Acad. Sci. U. S. A.*, 2017, **114**, 8138-8140.
29 P. J. Flory, *J. Chem. Phys.*, 1977, **66**, 5720-5729.
30 A. Kloczkowskif, J. E. Mark and B. Erman, *Macromolecules*, 1995, **28**, 5089-5096.
31 B. Erman and L. Monnerie, *Macromolecules*, 1989, **22**, 3342-3348.
32 A. M. Rumyantsev and J. J. de. Pablo, *Macromolecules*, 2020, **53**, 1281-1292.
33 C. M. Bates and F. S. Bates, *Macromolecules*, 2017, **50**, 3-22.
34 E. Helfand and Y. Tagami, *Polymer Letters*, 1971, **9**, 741-746.
35 J. Knebel, P. M. Geiger and E. Frey, *Phys. Rev. Lett.*, 2020, **125**, 258301.
36 J. D. Schieber, *J. Chem. Phys.*, 2003, **118**, 5162-5166.
37 G. G. Fuller, *Optical rheometry of complex fluids, topics in chemical engineering*, Oxford University Press, 1995.
38 L. Chen, T. L. Sun, K. P. Cui, D. R. King, T. Kurokawa, Y. Saruwatari and J. P. Gong, *J. Mater. Chem. A*, 2019, **7**, 17334-17344.
39 T. L. Sun, T. Kurokawa, S. Kuroda, A. B. Ihsan, T. Akasaki, K. Sato, M. A. Haque, T. Nakajima and J. P. Gong, *Nat. Mater.*, 2013, **12**, 932-937.

